Chemical Engineering Science 166 (2017) 246–261

Contents lists available at ScienceDirect

Chemical Engineering Science

journal homepage: www.elsevier.com/locate/ces

Rotary reverse flow reactor vs. adiabatic reactor with regenerative preheating - Design and comparison

Carlos D. Luzi *, Osvaldo M. Martínez, Guillermo F. Barreto

PROIRQ, Departamento de Ingeniería Química, Facultad de Ingeniería, UNLP, La Plata, Argentina
Centro de Investigación y Desarrollo en Ciencias Aplicadas "Dr. J. J. Ronco" (CINDECA) CCT La Plata, CONICET, UNLP, calle 47 No. 257, CP B1900AJK La Plata, Argentina

HIGHLIGHTS

- Two autothermal schemes for the treatment of VOCs are simulated and compared.
- Five different monolithic structures are considered for performance comparison.
- A design strategy is proposed considering a range of VOC content to be treated.
- The rotary reverse-flow reactor results more compact than the regenerator-reactor.
- The rotary reverse-flow reactor allows a more flexible operation.

ARTICLE INFO

Article history:
Received 7 October 2016
Received in revised form 25 February 2017
Accepted 18 March 2017
Available online 21 March 2017

Keywords:
Volatile organic compounds
Catalytic combustion
Regenerative heat exchange
Rotary reverse-flow reactor

ABSTRACT

The autothermal catalytic-combustion systems are commonly used for the purification of waste air streams contaminated with low concentrations of volatile organic compounds (VOC). Within this type of devices, the reverse flow reactors (RFR) are known to be more efficient than systems employing recuperative (surface) heat exchangers to preheat the waste air stream with the lean air effluent from the catalytic incinerator. The advantage of the RFR is basically due to the regenerative heat-exchange mechanism, provided by the inert and catalytic solids inside the unit.

As an alternative, the regenerative mechanism of preheating can be achieved by an independent heat exchanger, which coupled to a catalytic reactor could be expected to produce similar performance as the RFR.

In this context, this contribution is devoted to analyse comparatively the performances of a rotary reverse flow reactor (RRFR) and a system comprising a rotary regenerative heat-exchanger and a catalytic reactor (RHE-SR system) for the treatment of a waste air stream contaminated with ethanol and ethyl acetate, by means of mathematical simulation. Both alternatives are assumed to be composed of monoliths with square channels. A strategy of design for both systems suitable for their comparison is proposed, attending to a range of VOC concentration in the waste stream. Both alternatives can be regarded as being suitable options to carry out the target. However, the resulting designs show clear advantages in favour to the RRFR, as this alternative requires a significantly more compact equipment than the RHE-SR does and, besides, it allows to be operated under a wider range of the rotational speed, which is the main control variable once the systems are operating.

1. Introduction

In the last decades, the environmental regulations have become more stringent in many countries. As a result, research and development of technologies for the control of air contamination has grown considerably. Volatile organic compounds (VOCs) are the most common air contaminants and catalytic oxidation is the most widespread option among destructive alternatives, when the levels of VOCs are low – i.e., ≤1% – (Kolaczkowski, 2005).

Depending on the nature of each VOC and the catalyst used, common temperatures for the catalytic combustion ranges between 200 and 400 °C. Additionally, the waste air streams are usually at near ambient temperature and the flow rates are quite high. Therefore, the need to efficiently recover part of the

* Corresponding author at: PROIRQ, Departamento de Ingeniería Química, Facultad de Ingeniería, UNLP, La Plata, Argentina.
E-mail address: carlos.luzi@ing.unlp.edu.ar (C.D. Luzi).

http://dx.doi.org/10.1016/j.ces.2017.03.046
0009-2509/

Nomenclature

a	catalytic activity
a_0	catalytic activity of the fresh catalyst
a_{crit}	critical value of a for reactor extinction
a_v	specific interfacial area (m^2/m^3)
c_p	specific heat ($J\ kg^{-1}\ K^{-1}$)
C_j	molar concentration of the jth component in the gas phase (mol/m^3)
C_T	total molar concentration in the gas phase (mol/m^3)
D	diameter of the RRFR (m)
D_{RHE}	diameter of the regenerator (m)
D_R	diameter of the reactor (m)
d_h	hydraulic diameter of the channels (m) ($4\varepsilon_L/a_v$)
E_i	activation energy of the ith reaction ($J\ mol^{-1}\ K^{-1}$)
f_C	cleaning fraction
f_{cold}	fraction of the total cross-section of the regenerator used for the cooling step of the solid (m)
f_I	ratio of the length of the inert zone to the total length of the unit
G	superficial mass velocity ($kg\ m^{-2}\ s^{-1}$)
G_{mC}	cleaning mass flow rate ($kg\ s^{-1}$)
G_{mT}	total mass flow rate to be treated ($kg\ s^{-1}$)
h	heat transfer coefficient ($W\ m^{-2}\ K^{-1}$)
h^*	modified heat transfer coefficient (Eq. (9)) ($W\ m^{-2}\ K^{-1}$)
k_i	specific rate constant of the ith reaction (s^{-1})
$k_{i,ref}$	specific rate constant of the ith reaction, evaluated at T_{ref} (s^{-1})
K_j	adsorption constant of the jth component ($m^3\ mol^{-1}$)
$k_{m,j}$	mass transfer coefficient for the jth component ($m\ s^{-1}$)
ℓ	equivalent washcoat thickness (m) ($\delta_{cat}[1+\delta_{cat}/(L_{cell}-\delta_T)]$)
L	length of the RRFR (m)
L_{cell}	side of the unit cell of the monolith (m) ($N_{cell}^{-1/2}$)
L_{RHE}	length of the regenerator (m)
L_R	length of the reactor (m)
M_{air}	molecular weight of air
n	current half-cycle to be simulated
N_{cell}	number of cells per unit of cross-sectional area (m^{-2})
Nu	Nusselt number
r_i	ith reaction rate ($mol\ m^{-3}\ s^{-1}$)
$\mathbf{r}_j^{ef}$	effective rate of consumption of the jth component ($mol\ m^{-3}\ s^{-1}$)
R	ideal gas constant. ($J\ mol^{-1}\ K^{-1}$)
Re	Reynolds number (evaluated at feed conditions)
S	total cross-section of RRFR (m^2)
S_{RHE}	total cross-section of the regenerator (m^2)
S_R	total cross-section of the catalytic reactor (m^2)
Sh	Sherwood number
$\langle T_G\rangle^{RS}$	average temperature of the air stream at the output of the reaction step (K)
$\langle T_G\rangle^{cool}$	average temperature of the air stream at the output of the cooling step (K)
$\langle T_G\rangle^{C}$	average temperature of the air stream at the output of the cleaning step (K)
t	time (s)
$t_{\alpha 0}$	time at which a channel in the position α_0 at initial time (in the reaction step), reaches the cleaning step for the first time ($[(\pi-\varphi)-\alpha_0]t_{cycle}/(2\pi)$)
t_{cycle}	cycle period (s)
$t_{cycle}^{\min}$	minimum cycle period (s)
$t_{cycle,crit}$	critical cycle period (s)
$t_{cycle,low}$	minimum **operating** cycle time for the nominal operation (s)
t_{CS}	duration of a cleaning step (s)
t_{cool}	duration of a cooling step of the solid (s)
t_{reg}	duration of a heat regeneration step of the solid (RHE-SR) (s)
t_{RS}	duration of a reaction step (RRFR) (s)
T	temperature (K)
$T_G^{0,R}$	temperature of the air stream at the reactor inlet (K)
$T_G^{L_R,R}$	temperature of the air stream at the reactor outlet (K)
T_{ref}	reference temperature for the calculation of the kinetic coefficients (K)
$T_{S,\max}$	maximum temperature reached in the solid phase (K)
$T_{S,\max}^{adm}$	maximum allowable temperature in the solid phase used in the design (K)
V	total volume of the RRFR (m^3)
V_{RHE}	total volume of the regenerator (m^3)
V_R	total volume of the reactor (m^3)
W_{act}	total mass of the active material (kg)
W_I	total mass of the inert material (kg)
$X^{(n)}$	any of the variables T_S, T_G or $y_{j,G}$ for the nth half-cycle
$X_{ini}^{(n)}$	any of the variables T_S, T_G or $y_{j,G}$ at the beginning of the nth half-cycle
$X_{end}^{(n)}$	any of the variables T_S, T_G or $y_{j,G}$ at the end of the nth half-cycle
$\langle y_{j,G}\rangle^{RS}$	average mole fraction of the jth component in the gas phase at the output of the reaction step
$\langle y_{j,G}\rangle^{cool}$	average mole fraction of the jth component in the gas phase at the output of the cooling step
$\langle y_{j,G}\rangle^{C}$	average mole fraction of the jth component in the gas phase at the output of the cleaning step
$\langle y_{VOCs}\rangle$	average mole fraction of VOCs at the output
$y_{j,G}^{0,\min}$	minimum VOC concentration
$y_{j,G}^{0,nom}$	nominal VOC concentration
$y_{j,G}^{L_R,R}$	mole fraction of the jth component in the air stream at the output of the reactor
$\langle y_{VOCs}^{adm}\rangle$	allowable mole fraction of VOCs at the output
y_j	mole fraction of the jth component
z	axial position in the channel (m)

Greek letters

α_0	angular location of the channels at the operation start time
δ_{cat}	catalytic coating thickness (m)
δ_T	wall thickness (m)
ΔH_j	enthalpy of combustion of the jth component ($J\ mol^{-1}$)
$\lvert\Delta P\rvert$	pressure drop in a cycle (mbar)
$\lvert\Delta P\rvert^{adm}$	allowable pressure drop (absolute value) (mbar)
Δt_{oper}	difference between $t_{cycle,crit}$ and $t_{cycle,low}$ (s)
ΔT_{ad}	maximum adiabatic temperature rise (K)
ΔT^R	temperature rise in the reactor (K)
ε	void fraction of the bed
ε_T	tolerance for the maximum temperature (1 K)
ε_a	tolerance for the determination of the relative critical catalyst activity ($5\cdot10^{-4}$)
λ_S	thermal conductivity of the solid on the axial direction ($W\ m^{-1}\ K^{-1}$)
ρ	density ($kg\ m^{-3}$)
τ	time at which the channel just reaches the cleaning step
φ	angle span by the compartments discharging or collecting the cleaning stream

Subscripts

cat	catalyst-associated property
C	cleaning step

G	gas-phase-associated property or variable
i	ith reaction
I	inert-associated property or variable
S	property or variable associated with the solid phase or the interfacial area between the gas and solid phases

Superscripts

0	feed conditions
$0,R$	feed conditions to the reactor
ini	initial condition
L_R, R	outlet condition from the reactor

combustion energy of the processed gases by means of an autothermal scheme arises.

The simplest alternative consists in the utilization of a recuperative heat exchanger prior to a catalytic reactor, in order to achieve an autothermal operation. Nonetheless, due to the combination of high flow rates, low heat transfer coefficients and low adiabatic temperature rise, heat exchangers with large areas are needed. Within this context, the autothermal operation with regenerative heat transfer arises as a more efficient option.

One possibility is the use of a rotary heat exchanger (Willmott, 2002), in replacement of the recuperative one, prior to the adiabatic catalytic reactor, an alternative that will be identified as RHE-SR. This scheme operates under a regenerative mechanism of heat exchange, as the inert solids are cyclically heated and cooled by the inlet and outlet streams flowing counter-currently along stationary upper and lower compartments. After the start-up stage, the thermal behaviour of the regenerator follows periodically repeated cycles, i.e. a stage of *cyclic steady state* (CSS) is reached. The inert solids are arranged usually in a structured way, case that will be assumed here, and the gas streams then flow along the narrow channels inside the structure. The basic advantage is that a regenerative heat exchanger can be designed with a high area/volume ratio. At the same time, both recuperative and regenerative modes of heat exchange show similar operating features. Thus, the behaviour is completely equivalent when the regenerative heat exchanger operates at high enough rotational speed, as the inert solid temperature remains virtually constant. In addition, the variation of the rotational speed (i.e., the cycle time) modifies the heat exchange capacity, which allows controlling the inlet temperature of the reactor. Those aspects, besides the fact that rotary heat exchangers are currently available from commercial suppliers, make this system an attractive option.

Another alternative arises when the catalytic material is also mounted in the rotor as a middle section with inert material sections at both ends, which again perform a regenerative heat exchange function (Kolios et al., 2000). In principle, this system operates in the same way as the well-known conventional reverse-flow system (e.g. Chen et al., 2011; Marín et al., 2010; Matros and Bunimovich, 1996), in which the stationary inert and catalytic materials (in a structured or granular arrangement) are subject to periodically inversion of the flow direction of the gas. By this means, the whole rotor reaches a CSS with the central catalytic section at temperature levels required for the VOCs combustion, while the ends operate as preheating sectors. In practice, the reversal in the direction of the flow in the conventional reverse flow reactor (CRFR) is achieved by a valve system operated at a given switching time. A detailed description and discussion of the operation and simulation of the CRFR can be found on the well-known review of Matros and Bunimovich (1996), whereas an analysis of competitive alternatives and commercial applications can be found in the recent review by Zagoruiko (2012). On the other hand, in the rotary configuration (identified as rotary reverse flow reactor, hereinafter RRFR) the flow reversal occurs when the rotating channels enters either in the upper or in the lower compartment. The switching time is then determined by the rpm of the rotor. A comparison of both flow reversal devices, RRFR and CRFR, was carried out recently (Luzi et al., 2016). Although the behaviours of both alternatives are basically equivalent, some practical aspects were taken into account in the work of Luzi et al. (2016). Thus, a drawback of the CRFR is the emission of the untreated VOCs left in the entrance region of the bed (and in the pipeline) each time the flow is reversed, frequently referred to as wash-out problem. Instead, this effect can be removed in a rather simple way in the RRFR by installing an additional, small compartment, to sweep the remaining VOC with clean air before the flow reversal in the channels. Besides, practical recommendations allow the RRFR to be operated at lower switching times, a fact that enhances its heat exchange capacity. As a result, it was concluded that the RRFR represents a better option, based on the treatment of an air stream contaminated with ethanol and ethyl acetate (Luzi et al., 2016).

Comparison of different alternatives to eliminate VOCs through catalytic oxidation has been addressed by several authors. It should be mentioned the work of Matros et al. (1994), in which a conventional reverse flow reactor with inert ends is compared with the operation of the three beds with flow reversal on the inert beds only. The catalytic bed operates under unsteady state, as a consequence of variable feed conditions. Fissore and Barresi (2002) have compared a network of two or three reactors simulating a moving bed (or ring reactor) with a conventional reverse-flow reactor.

The objective pursued in this contribution is to compare the performance of the RRFR against the RHE-SR, which, as discussed in the previous paragraphs, is conceptually simpler than the RRFR. Both systems introduce a regenerative mechanism of heat exchange through a rotary device. From this point of view they can be expected to behave similarly. However, for both setups proposed in the present contribution there is an important difference that motivates the comparison: the catalytic reactor in the RHE-SR system operates strictly in steady state (once the regenerator reaches the CSS) and does not participate in the heat regeneration mechanism, while the catalytic section in the RRFR is also involved in the CSS and can still participate in the regenerative mechanism of heat exchange.

To accomplish the proposed comparison, the elimination of an ethanol and ethyl acetate mixture on a waste air stream is again employed as a case study. Monolithic structures with square channels are assumed for both systems and five configurations of the monolith cell are considered in order to select the most suitable one for each of the alternatives, RHE-SR and RRFR. The sizing and comparison of both units is carried out by considering a number of issues that can be encountered in many practical examples of VOC treatment. First, a variable level of operating VOC content is taking into account. Second, the capability of both setups to cope with catalytic ageing and the operative flexibility, as reflected by the range of cycle time to maintain ignited conditions, are evaluated. The same carefully chosen attributes and requirements for both systems are used to avoid masking the intrinsic differences between them.

2. Case study

The catalytic incineration of ethyl acetate and ethanol over Mn and Cu oxides (Morales et al., 2008) in an air stream has been

Table 1
Characteristics of the VOC-laden air stream.

Mass flow rate (kg s^{-1})	Pressure (bar)	Temperature (°C)	Minimum composition (ppmV)		Nominal composition (ppmV)	
			EA	Et	EA	Et
12.7	1.06	50	307 (ΔT_{ad} = 27 °C)	125	615 (ΔT_{ad} = 54 °C)	250

chosen as the case-study. Those compounds are used as solvents in printing processes and are typical VOC released by the manufacture of packaging. Table 1 presents the specific characteristics of the waste stream. In practice, the VOC concentration in the air stream can vary due to variable operating conditions in the primary processes. Therefore, for the study here described it was assumed that the treatment of the waste stream should cope with VOC concentrations ranging from a nominal to a minimum level, as defined in Table 1. Values of the maximum adiabatic temperature rises, ΔT_{ad}, are also given in Table 1.

Campesi et al. (2012a, 2012b) have studied the combustion of ethyl acetate and ethanol, showing that the later produces acetaldehyde as an intermediate. The reactions and kinetic expressions involved –identified by indices 1, 2, and 3 for ethyl acetate, ethanol, and acetaldehyde, respectively– are:

$$C_4H_8O_2 + 5\ O_2 \rightarrow 4\ CO_2 + 4\ H_2O$$

$$C_2H_6O + 1/2\ O_2 \rightarrow C_2H_4O + H_2O$$

$$C_2H_4O + 5/2\ O_2 \rightarrow 2\ CO_2 + 2\ H_2O$$

$$r_i = \frac{k_i C_i}{1 + K_1 C_1 + K_3 C_3} \quad \text{for } i = 1 \ldots 3 \tag{1}$$

$$k_i = k_{i,ref} \exp\left[-\frac{E_i}{R}\left(\frac{1}{T} - \frac{1}{T_{ref}}\right)\right] \quad \text{for } i = 1 \ldots 3 \tag{2}$$

The intrinsic values of the kinetics parameters are summarizes in Table 2 (Campesi et al., 2012b).

2.1. Description of both autothermal schemes, RRFR and RHE-SR

The scheme of the RRFR studied by (Luzi et al., 2016) is shown in Fig. 1, where the rotor in which inert and catalytic monoliths are mounted can be identified. The waste stream is split and enters the unit from the chambers at the left and right sides of the rotor. The cleaning streams allow avoiding the wash-out problem mentioned in Section 1, and it is assumed in Fig. 1 that they are small diversions from the effluent streams already treated. The chambers are segmented by two longitudinal plane baffles rotated a small angle φ around the axis. Thus, four compartments can be identified in each chamber. Two of them, defined by the angle φ, allow a cleaning stream either to enter or to exit the rotor, and two large compartments, defined by an angle (π-φ), allow one half of the waste stream to enter the rotor and one half of the treated stream to exit the rotor.

In this way, during one turn each channel in the upper half of the rotor (see Fig. 1) is first fed by the waste stream with the flow direction from left to right, defining a *reaction step*. Afterwards, it receives the cleaning stream, with the same flow direction, defining a *cleaning step*. This is followed by a second reaction step and a second cleaning step that takes place in the lower half of the rotor with the flow reversed (i.e., from right to left), to complete the turn.

Assuming that heat conduction in the monolithic matrices can be neglected in the transverse directions and that each channel receives a constant flow during a reaction or a cleaning step, the behaviour of all the channels aligned on a radial direction will be the same. At these conditions, the RRFR is equivalent to a conventional flow-reverse system operated by valves, except for the presence of the cleaning steps.

Luzi et al. (2016) suggested limiting the rotational speed in a RRFR to usual values in rotary heat exchangers: 2 to 10 rpm. Thus, the cycle time, t_{cycle}, can be as low as 6 s. Given a value of t_{cycle}, the duration of each reaction step and each cleaning step, t_{RS} and t_{CS}, is evaluated as:

$$t_{RS} = (1 - f_C) t_{cycle}/2, \tag{3}$$

$$t_{CS} = f_C t_{cycle}/2, \tag{4}$$

where f_C is the fraction (φ/π) of the total section of the rotor in contact with the cleaning streams (hereafter referred to as *cleaning fraction*).

Fig. 2 shows schematically a RHE-SR. The chambers at both sides of the rotary heat exchanger are segmented by a longitudinal baffle extended from side to side of the shell and a second baffle, at a small angle φ with respect to first one, extended from one side of the shell up to the axis. The compartments spanning the angle φ allow the circulation of the cleaning stream, which in Fig. 2a is assumed to be driven by an independent blower (alternatively, the cleaning stream can be a diversion of the exit stream from the reactor, in a similar way as described for the RRFR). The compartments spanning the angle (π − φ) (the upper compartments in Fig. 2) are set apart for the circulation of the waste stream and the lower compartments spanning an angle π are set apart for the circulation of the stream coming from the catalytic reactor.

During one turn each channel in the rotor is first fed and cooled by the waste stream (*cooling step*), then it receives the cleaning stream (*cleaning step*), and finally it receives from the opposite direction the hot stream from the reactor (*heat regeneration step*).

For defining the cycle time, t_{cycle}, in the regenerator, the range 2–10 rpm will also be considered. The duration of the cooling, cleaning and heat regeneration steps are related to t_{cycle} in the following way:

Table 2
Kinetic parameters.

Pre-exponential factor (s^{-1})		Activation energy (J mol^{-1})		Reference temperature (K) and adsorption constant (m^3 mol^{-1})	
$k_{1,ref}$	$6.62 \cdot 10^1$	E_1	$1.48 \cdot 10^5$	T_{ref}	448
$k_{2,ref}$	$1.81\ 10^3$	E_2	$1.10\ 10^5$	K_1	$4.19\ 10^1$
$k_{3,ref}$	$1.22\ 10^1$	E_3	$1.69\ 10^5$	K_3	$6.75\ 10^1$

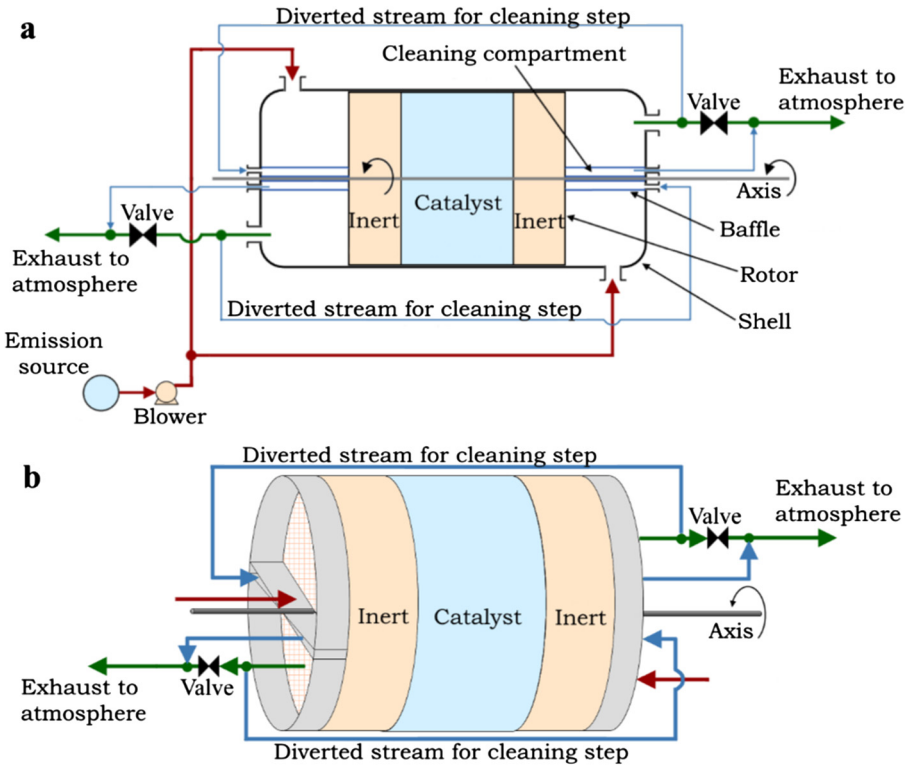

Fig. 1. (a) Scheme of the rotary reverse-flow reactor (RRFR) and (b) detail of the rotor. The valve (►◄) is actuated to allow the diverted flow into the cleaning step.

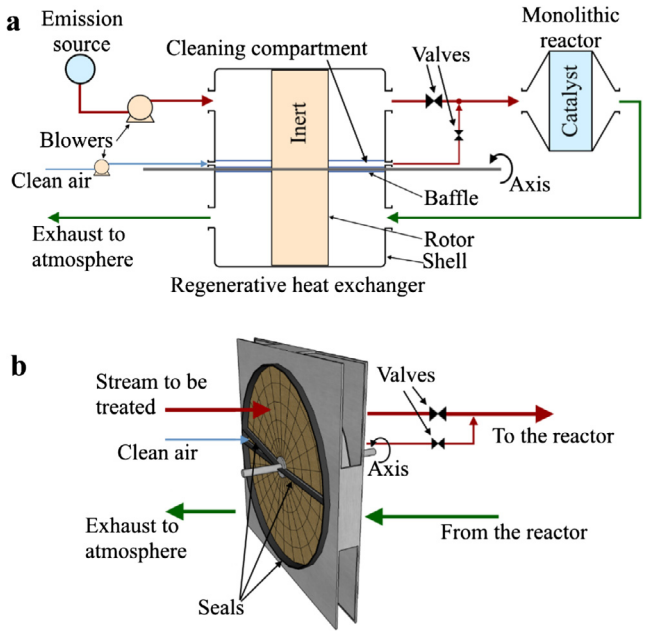

Fig. 2. (a) Scheme of the system formed by the rotary heat exchanger and the catalytic reactor (RHE-SR) and (b) detail of the rotor of the regenerative heat exchanger.

$$t_{cool} = f_{cool} t_{cycle}, \tag{5}$$

$$t_{CS} = f_C t_{cycle}, \tag{6}$$

$$t_{reg} = (1 - f_{cool} - f_C) t_{cycle}, \tag{7}$$

where $f_{cool} = (\pi - \varphi)/(2\pi)$ and $f_C = \varphi/(2\pi)$ are the fractions of the total cross-section of the rotor in contact with the cleaning and waste streams, respectively.

Once the operation of the regenerator reaches the CSS, the upper right compartment in Fig. 2 receives the discharge of all channels and the properties of the resulting mixture will be constant. Therefore, the catalytic reactor (Fig. 2) is fed with a stationary stream and will operate strictly under steady state conditions.

As already mentioned, both systems, RHE-SR and RRFR, are assumed to be monolithic structures. The catalytic reactor of the RHE-SR system and the reaction section in the RRFR comprise an inert matrix and a 10 μm thick uniform catalytic coating, δ_{cat}. For the sizing of the units a set of 5 types of square cells, whose characteristics are shown in Table 3, were considered in order to select the most adequate for each system. The dimensions in Table 3 include the catalytic coating. The first three of them correspond to commercial standards of Corning Incorporated (Boger et al., 2004) with 200, 400, and 600 cells per square inch and wall thicknesses of 12.5, 7.5, and 4.0 thousandths of an inch, respectively. Configurations 4 and 5 are modifications of configurations 2 and 3, respectively, with a thicker wall leading to the same void fraction as that of configuration number 1. The properties of solid structure are evaluated as those of nonporous cordierite (Gulati, 2005). The cells of the inert ends of the RRFR and the regenerative heat exchanger of the RHE-SR are assumed to be the same as those of the catalytic counterpart, but just built of inert material.

3. Modelling

For both alternatives, RRFR and RHE-SR, a heterogeneous one-dimensional model has been employed, without the explicit inclusion of axial dispersion terms. The model and the assumptions made were those described by Luzi et al. (2016) for the RRFR, although they are included here for the sake of completeness.

The overall accumulation of mass in the gas phase, eventual homogeneous gas-phase reactions, and energy losses have been neglected. In addition, the inert material was assumed to be

Table 3
Cell configurations and relevant geometrical properties.

No.	$10^{-5}N_{cell}$ (m^{-2})	$10^{4}\delta_T$ (m)	ε	a_v (m^{-1})	$10^{3}d_h$ (m)
1	3.1	3.18	0.678	1833	1.48
2	6.2	1.91	0.722	2677	1.08
3	9.3	1.02	0.814	3480	0.94
4	6.2	2.25	0.678	2593	1.05
5	9.3	1.83	0.678	3176	0.85

non-adsorbent and pseudo steady state was employed to evaluate the effective reaction rates in the catalytic layer.

The physical properties of the waste stream were considered as those of pure air, owing to the low concentration of VOCs (below 1%), assuming ideal gas behaviour for the gas phase. Additionally, the variation in the total molar flow rate due to the chemical reactions was neglected.

Laminar flow holds in the channels of the monolithic for all conditions considered in this work. Then, the pressure drop in the square channels was calculated by considering that the product of the friction factor and Reynolds number equals 14.2. As the pressure drop along the monolith turned out to be very low as compared to the absolute pressure, pressure was assumed uniform for solving the energy and mass conservation equations.

It is expected that most of the hypothesis described in the previous paragraphs will be satisfied at typical operating conditions in full scale incineration units. However, specific situations cannot be ruled out. For example, due to the dynamic behaviour of the RRFR, the assumption of negligible accumulation of species on the surface of the catalyst pores may need reconsideration when certain species are strongly adsorbed on the catalyst internal surface. In these cases, accumulation terms for such species should be considered in the model. In addition, if the adsorption-desorption steps for such species are not fast enough, the rates of consumption/production of each compound will be different to that predicted when the catalyst layer is considered to be in a (pseudo) steady state.

Finally, the inlet stream was considered to be evenly distributed in the available channels. For both rotors (the whole RRFR and the regenerator in the RHE-SR), the thermal conduction on the transverse directions was additionally neglected. These assumptions enable to formulate the same energy and mass balance conservation equations for any channel of the rotor. The validity of both assumptions, uniform flow distribution and negligible thermal conduction on the transverse directions, are further discussed in Appendix A.

3.1. Modelling of the RRFR

According to the previous assumptions, for the catalytic zones of the RRFR, the following energy and mass balances were applied to simulate its behaviour, during the rotation of a given channel:

Energy balance in the solid phase:

$$(1-\varepsilon)(\rho c_p)_S \frac{\partial T_S}{\partial t} = a_v h^*(T_G - T_S) + a_v \ell \sum_{j=1}^{3}(-\Delta H_j)\mathbf{r}_j^{ef} \tag{8}$$

where $\ell = \delta_{cat}[1 + \delta_{cat}/(L_{cell} - \delta_T)]$ is the equivalent washcoat thickness (ratio of the volume of catalytic washcoat to the total transfer area), $L_{cell} = N_{cell}^{-1/2}$ is the side of the unit cell of the monolith, and h^* is a modified heat transfer coefficient that approximately accounts for the effect of axial thermal conduction of the solid material through an adaptation of the expression proposed by Vortmeyer and Schaefer (1974),

$$\frac{1}{h^*} = \frac{1}{h} + \frac{a_v(1-\varepsilon)\lambda_S}{(Gc_{pG})^2} \tag{9}$$

Energy balance in the gas phase:

$$\varepsilon(\rho c_p)_G \frac{\partial T_G}{\partial t} = -Gc_{pG}\frac{\partial T_G}{\partial z} - a_v h^*(T_G - T_S) \tag{10}$$

Mass balance for each component in the gas phase:

$$\varepsilon\frac{\partial(C_T y_{j,G})}{\partial t} = -\frac{G}{M_{air}}\frac{\partial y_{j,G}}{\partial z} - a_v k_{mj} C_T(y_{j,G} - y_{j,S}) \quad j = 1,2,3 \tag{11}$$

Mass balance for each component in the solid phase:

$$k_{mj}C_T(y_{j,G} - y_{j,S}) - \ell\mathbf{r}_j^{ef} = 0 \quad j = 1,2,3 \tag{12}$$

In the end zones, where only inert material is present, Eq. (12) does not apply whereas the same balances given by Eqs. (8)–(11) apply after dropping the reaction-heat terms in Eq. (8) and the mass transfer term in Eq. (11).

In Eqs. (9)–(11) the superficial mass velocity G in a reaction step is given by $G = G_{mT}/[S(1 - f_C)]$, where G_{mT} is the mass flow rate of the waste stream and S is the total cross-section of the rotor, and in a cleaning step $G = G_{mC}/(f_C S)$, where G_{mC} is total mass flow rate employed for cleaning.

The mass and heat transfer coefficients are calculated from *Sh* and *Nu* numbers at conditions of constant surface concentration/temperature in laminar flow. The asymptotic values for a square channel are $Sh = Nu = 2.977$. However, entrance effects could be significant in laminar flow and, in practice, monolithic structures are assembled by piling modules of predefined length, a feature that repeats those effects. Then, a channel length of 0.25 m was considered and a spatial average value of *Sh* and *Nu* was used, as described by Luzi (2015). The corrected values of *Sh* and *Nu* differed in no more than 5%. Also, for ceramic materials, in particular for the cordierite assumed in this work, the solid thermal conductivity λ_S is low enough to make negligible (less than 1%) the correction to h according to Eq. (9). Therefore, it can be concluded that the asymptotic values $Sh = Nu = 2.977$ could have been employed without any significant practical consequence.

The effective reaction rate for each component is calculated from the approximation proposed by Campesi et al. (2012a), by employing the effective diffusivities reported in that work and the equivalent washcoat thickness ℓ.

3.1.1. Boundary and initial conditions for the RRFR and solution for the CSS

Under the assumptions discussed in Section 3, it can be concluded that each channel of the RRFR will show the same behaviour once the CSS is reached. However, the evolution of temperatures and concentrations in the channels from the initial conditions (even when these conditions were the same for all channels) will follow different paths. To visualize this fact, consider at the operation start time (by rotating the bed and allowing the incoming flow of VOC laden air) the channels facing the upper compartment in Fig. 1, which discharges one half of the waste stream. These channels will be distributed on angles α_0 varying from zero to the compartment angle $(\pi - \varphi)$, and initiate the operation in a reaction step. However, they will reach the next compartment (discharging the cleaning stream) at different times,

$t_{\alpha 0} = [(\pi - \varphi) - \alpha_0]t_{cycle}/(2\pi)$, and therefore they will begin the cleaning step with different temperature and concentration profiles. The differences will be maintained as the operation evolves, but they will be progressively fading away as the CSS is approached. As we are just interested in the CSS, only the evolution of a single (test) channel, initially at the beginning of a reaction step, with $\alpha_0 = 0$, will be evaluated to represent the whole set once the CSS is reached. To this end some arbitrary initial conditions are chosen for the test channel. The transient behaviour of the test channel is then evaluated until concentration and temperature variations during a cycle remain virtually unchanged in the next cycle, considering the initial and boundary conditions described in the following paragraphs.

The initial conditions were chosen as $y_{j,G}(0,z) = 0$ (clean air) and $T_S(0,z) = T_G(0,z) = T^{ini}$, where the value $T^{ini} = 350\,^{\circ}C$ always allowed to reach, when feasible, the ignited CSS. When the test channel just reaches the next cleaning step, it keeps the temperature and concentration profiles evaluated at the end of the reaction step. In a similar way, when the test channel leaves the cleaning step to begin a new reaction step, the temperature and concentration profiles are maintained, but to keep on working with positive values of G in Eqs. (8)–(12), the coordinate z is reversed. That is, defining $X^{(n)}$ as any of the state variables T_S, T_G or $y_{j,G}$ for the n-th half-cycle ($n \geqslant 2$):

$$X_{ini}^{(n)}(z) = X_{end}^{(n-1)}(L - z), \tag{13}$$

where $X_{ini}^{(n)}$ is the value of X at the beginning of the current half-cycle (i.e., in the beginning of a reaction step) and $X_{end}^{(n-1)}$ is the value of X at the end of the previous half-cycle (i.e., at the end of the previous cleaning step).

With respect to the boundary conditions, for $z = 0$, they are determined by the feed conditions in the corresponding compartment. Thus, in a reaction step, the test channel receives the waste stream at constant temperature and composition, $T_G(t,0) = T_G^0$ and $y_{j,G}(t,0) = y_{j,G}^0$ (see Table 1). On the contrary, during a cleaning step the test channel is fed by a fraction of the cleaned air stream (see Fig. 1), characterized by a temperature and composition $\langle T_G \rangle^{RS}$ and $\langle y_{j,G} \rangle^{RS}$. In general, $\langle T_G \rangle^{RS}$ and $\langle y_{j,G} \rangle^{RS}$ are the result of mixing the discharges of all channels operating simultaneously in a reaction step. In the CSS, these values are independent of time, but during the actual evolution they will be time-dependant and, furthermore, they will depend on the evolution of all channels. Therefore, as we only follow the evolution of the test channel, a simplification has to be made. That is, the values of $\langle T_G \rangle^{RS}$ and $\langle y_{j,G} \rangle^{RS}$ are estimated from averaging the temperature and concentration of the discharge of the test channel in its journey from the previous reaction step. Thus, denoting τ the time at which the channel just reaches the cleaning step, the following expressions allow evaluating $\langle T_G \rangle^{RS}$ and $\langle y_{j,G} \rangle^{RS}$:

$$\langle y_{j,G} \rangle^{RS} = \frac{1}{t_{RS}} \int_{\tau - t_{RS}}^{\tau} y_{j,G}(t,L)dt, \tag{14}$$

$$t_{RS} \int_{T_0}^{\langle T_G \rangle^{RS}} c_{pG}(T)dT = \int_{\tau - t_{RS}}^{\tau} \left[\int_{T_0}^{T_G(t,L)} c_{pG}(T)dT \right] dt, \tag{15}$$

where t_{RS} is given in Eq. (3). During the journey of the test channel in a cleaning step, $\tau < t < \tau + t_{CS}$ (see Eq. (4) for t_{CS}), the values of $\langle T_G \rangle^{RS}$ and $\langle y_{j,G} \rangle^{RS}$ from Eqs. (14) and (15) define the constant conditions assumed at the channel inlet. As Eqs. (14) and (15) do provide the correct values of $\langle T_G \rangle^{RS}$ and $\langle y_{j,G} \rangle^{RS}$ at the CSS, the evolution of the test channel will be approximated, but the CSS will be correctly evaluated.

Additionally, on consideration of the model proposed, at the boundary between the inert and catalytic zones, the values of temperature and mole fractions in the gas phase are required to be continuous.

Regarding the mass flow rate of the cleaning stream, it must be emphasized that the value selected should allow the complete displacement of the volume of air contaminated with VOCs in the inlet zone of the channels after the cleaning time t_{CS}. Thus, the minimum mass flow rate diverted for the cleaning step is chosen in order to guarantee that the total volume of contaminated air reached the hot catalyst during this step, as detailed by Luzi et al. (2016).

Finally, for solving the set of partial differential-algebraic equations, Eqs. (8)–(12), the spatial variable z is discretized by taking 150 intervals, and the spatial derivatives are approximated by a second-order backward finite difference scheme. In this way, the original system becomes reduced to a system of ordinary differential-algebraic equations (DAEs) in the time variable. The backward approximation enables that the DAEs at any axial position z do not depend on the values of upwards variables. This feature permits a successive temporal solution from the first up to the final spatial node (at $z = L$). In each step, conventional routines of solution for DAEs are employed. The evolution from initial conditions until the CSS can be evaluated in this way. However, an algorithm for accelerating the convergence to the CSS, based on the results at the end of successive half-cycles, has been employed and described by Luzi (2015). Depending on the cycle time and operating conditions, a total of 10–20 iterations had usually been required. In this way, the algorithm for accelerating the convergence allowed to decrease the number of iterations and the computing time by a factor of about 5 and 4, respectively.

3.2. Modelling of the RHE-SR

Under the assumptions discussed at the beginning of Section 3, the conservation equations for any channel of the rotary regenerator will be equivalent to Eqs. (8)–(11), although with $r_j^{ef} = 0$ in Eq. (8), and with the mass transfer terms dropped in Eq. (11). Besides, Eqs. (12) do not apply. Thus, the governing equations become:

Energy balance in the solid phase (regenerator):

$$(1 - \varepsilon)(\rho c_p)_S \frac{\partial T_S}{\partial t} = a_v h^* (T_G - T_S) \tag{16}$$

Energy balance in the gas phase (regenerator):

$$\varepsilon(\rho c_p)_G \frac{\partial T_G}{\partial t} = -G c_{pG} \frac{\partial T_G}{\partial z} - a_v h^* (T_G - T_S) \tag{17}$$

Mass balance for each component in the gas phase (regenerator):

$$\varepsilon \frac{\partial (C_T y_{j,G})}{\partial t} = -\frac{G}{M_{air}} \frac{\partial y_{j,G}}{\partial z} \quad j = 1,2,3 \tag{18}$$

In Eqs. (17) and (18) the superficial mass velocity is $G = G_{mT}/(f_{cool} S_{RHE})$ in the cooling step, where S_{RHE} is the total cross-section of the rotor, $G = G_{mC}/(f_C S_{RHE})$ in the cleaning step, and $G = (G_{mT} + G_{mC})/[S_{RHE}(1 - f_{cool} - f_C)]$ in the heat regeneration step.

As for the RRFR, the simulation just aims at evaluating the CSS of the regenerator. It was discussed in Section 2.1 that the catalytic reactor will operate at steady state conditions when the CSS is reached in the regenerator. Therefore, the model used for the reactor only accounts for the steady state, i.e. a model without accumulation terms. Besides, the assumption of uniform flow distribution enables us to simulate just a single channel of the catalytic monolith. Thus, the conservation equations in this channel are written as follows:

Energy balance in the gas phase (reactor):

$$Gc_{pG}\frac{dT_G}{dz} = -a_v h^*(T_G - T_S) \tag{19}$$

Mass balance for each component in the gas phase (reactor):

$$\frac{G}{M_{air}}\frac{dy_{j,G}}{dz} = -a_v k_{m,j} C_T (y_{j,G} - y_{j,S}) \quad j = 1,2,3 \tag{20}$$

Energy balance in the solid phase (reactor):

$$a_v h^*(T_G - T_S) + a_v \ell \sum_{j=1}^{3}(-\Delta H_j)\mathbf{r}_j^{ef} = 0 \tag{21}$$

Mass balance for each component in the solid phase (reactor):

$$k_{m,j} C_T (y_{j,G} - y_{j,S}) - \ell \mathbf{r}_j^{ef} = 0 \quad j = 1,2,3 \tag{22}$$

In Eqs. (19) and (20), $G = (G_{mT} + G_{mC})/S_R$, where S_R is the total cross-section area of the reactor.

Mass and heat transfer coefficients and effective reaction rates were evaluated in the same way as for the simulation of the RRFR.

3.2.1. Boundary and initial conditions for the RHE-SR and solution for the CSS

A single (test) channel has been again considered for evaluating the CSS in the regenerator. The test channel is assumed to start the operation at the beginning of the cooling and initial conditions given by $y_{j,G}(0,z) = 0$ (clean air) and $T_S(0,z) = T_G(0,z) = T^{ini}$, with $T^{ini} = 300$ °C.

When the channel just begins a new step, it keeps the concentration and temperature profiles reached at the end of the previous one. If the new step involves a flow reversal (i.e., from a heat regeneration step to a cooling step or from a cleaning step to a heat regeneration step), the coordinate z is reversed and values of the state variables reassigned according to Eq. (13).

The boundary conditions at $z = 0$ during the cooling step are $T_G(t,0) = T_G^0$ and $y_{j,G}(t,0) = y_{j,G}^0$ (i.e. the values in the waste stream, see Table 1), during the cleaning step $T_G(t,0) = T_G^0$ and $y_{j,G}(t,0) = 0$ (i.e. values for clean air at the same temperature as in the waste stream), and during the heat regeneration step $T_G(t,0) = T_G^{L_R,R}$ and $y_{j,G}(t,0) = y_{j,G}^{L_R,R}$, where $T_G^{L_R,R}$ and $y_{j,G}^{L_R,R}$ are the temperature and mole fractions at the catalytic reactor exit, evaluated as described next.

After the test channel of the regenerator has completed successively a cooling step and a cleaning step, the exit values of concentrations and temperature are averaged on t_{cool} and t_{CS}, respectively, using expressions similar to Eqs. (14) and (15). The average values are denoted $\langle y_{j,G}\rangle^{cool}$, $\langle T_G\rangle^{cool}$ for the cooling step, and $\langle y_{j,G}\rangle^{C}$, $\langle T_G\rangle^{C}$ for the cleaning step. These values are assumed to correspond to the conditions of the exit streams from the cooling and cleaning compartments and, in turn, their mixture determines the conditions at the entrance of the catalytic reactor, $y_{j,G}^{0,R}$ and $T_G^{0,R}$:

$$y_{j,G}^{0,R} = \frac{G_{mT}}{G_{mT}+G_{mC}}\langle y_{j,G}\rangle^{cool} + \frac{G_{mC}}{G_{mT}+G_{mC}}\langle y_{j,G}\rangle^{C} \tag{23}$$

$$G_{mT}\int_{\langle T_G\rangle^{cool}}^{T_G^{0,R}} c_{pG}(T)dT + G_{mC}\int_{\langle T_G\rangle^{C}}^{T_G^{0,R}} c_{pG}(T)dT = 0 \tag{24}$$

The cleaning mass flow rate G_{mC} is evaluated as 10% larger than the value needed to displace the mass of gas held in the test channel when it just initiates a cleaning step:

$$G_{mC} = 1.1\frac{\varepsilon f_C S_{RHE}}{t_{CS}}\int_0^{L_{RHE}} \rho_G dz = 1.1\frac{\varepsilon S_{RHE}}{t_{cycle}}\int_0^{L_{RHE}} \rho_G dz, \tag{25}$$

where L_{RHE} is the length of the regenerator and ρ_G is the air density evaluated at the time the test channel just initiates a cleaning step. In the second equality, t_{CS} has been replaced according to Eq. (6).

It is recalled that values $y_{j,G}^{0,R}$ and $T_G^{0,R}$ evaluated from Eqs. (23) and (24) do not strictly correspond to the start-up stage, but they apply correctly once the CSS of the regenerator is reached. At this point, two alternatives for the determination of the CSS can be identified, which are described in the following paragraphs.

Alternative 1: From the initial conditions, the steady state of the whole system can be determined in a similar way as that employed for the RRFR. Thus, after the simulation of the cooling step and cleaning step has been completed for the test channel of the regenerator, values of $y_{j,G}^{0,R}$ and $T_G^{0,R}$ are obtained. Then, the simulation of the catalytic reactor provides the boundary conditions for the heat regeneration step, i.e. the exit values of temperature and composition of the reactor, $T_G^{L_R,R}$ and $y_{j,G}^{L_R,R}$. These allow simulating the next heat regeneration step. The computation process is continued until the CSS in the regenerator is reached.

Alternative 2: For guessed values of $T_G^{L_R,R}$ and $y_{j,G}^{L_R,R}$, it is possible to determine the CSS of the regenerator "independently" by regarding that these values remain fixed. When this task is accomplished, values of $y_{j,G}^{0,R}$ and $T_G^{0,R}$ will become available and a simulation of the catalytic reactor is carried out with them, which will render new values of $T_G^{L_R,R}$ and $y_{j,G}^{L_R,R}$. The procedure is repeated until successive values of $T_G^{L_R,R}$ and $y_{j,G}^{L_R,R}$ remain virtually unchanged.

For either alternative, 1 or 2, it is noted that in evaluating the CSS of the regenerator through Eqs. (16)–(18), the same strategy as that used for the RRFR were employed, regarding the spatial discretization and the algorithm for accelerating the convergence.

At this point, it should be noted that when an ignited steady state in the catalytic reactor is feasible, the VOC concentrations at the reactor outlet are of the order of 1 ppm or less, as will be further discussed later. Therefore, the temperature rise of the gas stream from the reactor inlet to outlet, ΔT^R, practically equals the adiabatic temperature rise ΔT_{ad} (strictly for full conversion, $\Delta T^R = \Delta T_{ad}$). Then, the use of the second alternative just described is strongly suggested, but instead of employing $T_G^{L_R,R}$ as the iteration variable to evaluate the CSS of the regenerator, it is convenient to use ΔT^R, as they are related by $T_G^{L_R,R} = T_G^{0,R} + \Delta T^R$. The iterative process is initiated with guess values $\Delta T^R = \Delta T_{ad}$ and $y_{j,G}^{L_R,R} = 0$, and the iterations are stopped when successive values of ΔT^R will not differ significantly. If the ignited steady is feasible, this will normally happen after a couple of iterations. The second iteration is mainly needed as ΔT_{ad} is updated to account for its slight dependence on $T_G^{0,R}$. Instead, when the ignited steady state is not feasible, a decreasing sequence of values of ΔT^R will reveal this situation. Actually, $\Delta T^R \to 0$ in this case, but the iterations can be stopped before reaching the null limiting value.

The advantage of the procedure just outlined when the ignited steady state holds is that only one or two simulation of the catalytic reactor will be necessary, a fact that will allow saving an important amount of calculations, particularly if the evaluation of effective reaction rates in the catalytic washcoat requires iterative calculations.

Finally, it should be mentioned that for the use of the alternative 2, there are approximations to evaluate the CSS of the regenerator, which avoid the numerical solution of the partial differential equations. The approximation described by Thulukkanam (2013), in terms of the classical ε-NTU method, was tried. Very reasonable results were obtained in this way for the cases tested, with differences less than 10 °C in the predicted temperatures at the reactor inlet and outlet. In this way the evaluation of the RHE-SR

system can be sped out even more, and the algorithm for solving the differential equations avoided. Nonetheless, the results here presented were obtained by the numerical procedure described by the alternative 2 using ΔT^R as the iteration variable, as computing was not a critical issue, the presence and effects of the cleaning step can be accounted for, and pointwise thermo-physical properties can be evaluated in the regenerator. Depending on the cycle time and operating conditions, for each guess value of ΔT^R, a total of 7–15 iterations for reaching the CSS of the regenerator had been required.

4. Design and operation of the RRFR

A design strategy for the RRFR, applied to a waste stream with the characteristics defined in Table 1 was presented by Luzi et al. (2016), while the monolith cell #5 was chosen as the best alternative from the list in Table 3, according to the criteria explained by Luzi (2015). Only the relevant aspects involved in the design of the RRFR, which concern the purpose of the present contribution, will be discussed below.

The leading requirement for a VOC abatement system is the emission limit value set by the regulations. The "Directive 2010/75/EU" (2010) of the European Commission has been considered. Taking into account the type of VOC and the type of industrial activity, the maximum VOC concentration allowed in the atmospheric discharge is 20 mgC/Nm^3, which corresponds to values between 9 and 20 ppmV, depending on the ratio of the ethyl acetate to the ethanol in the discharge. Nonetheless, values of concentrations in that range are not adequate as a design requirement since the system will operate close to the extinction when any variable is changed. Therefore, for the VOC concentration at the reactor outlet, a value $\langle y^{adm}_{VOCs}\rangle = 1$ ppmV was established. As high temperatures increase the combustion rates, this target was imposed to the operation with minimum VOC concentration (Table 1). Also, as short cycle times increase the heat exchange capacity of the unit, the minimum size will arise when the unit is operated at the minimum allowed cycle time $t^{\min}_{cycle}$. To set this value, the usual range in rotary heat exchangers (2–10 rpm) was considered and a conservative value $t^{\min}_{cycle} = 30$ s (i.e. for 2 rpm) was adopted. Once a monolith cell is chosen and the depth of the catalytic washcoat established, the reaction rates per unit volume of the monolith becomes independent of the length/diameter ratio of the rotor. Also, as noted in Section 3.1, the asymptotic values of mass and heat transfer coefficients are suitable for the calculations and since they do not depend on the linear fluid velocity, the heat and mass transfer processes becomes also independent of the ratio length/diameter. Consequently, the total volume of the rotor necessary to satisfy $\langle y^{adm}_{VOCs}\rangle = 1$ ppmV is virtually independent of the length/diameter ratio.

Both ends of the RRFR are intended to preheat the waste stream and consequently they operate over $t^{\min}_{cycle}$ at average temperatures below the level necessary to attain significant reaction rates, which roughly can be evaluated in the range 175–200 °C for the most refractory species, acetaldehyde and ethyl acetate (Campesi et al., 2012b), in this study. Then, the value of the inert fraction f_I was chosen so that at the boundaries between the inert and central catalytic zones the average temperature is nearly 190 °C. In this way, a value $f_I = 0.5$ was adopted.

The length/diameter ratio was chosen to operate the unit at conditions of nominal VOC concentration (when higher temperatures arise) with an overall pressure drop of $|\Delta P|^{adm} = 50$ mbar, assumed to be the pressure rise provided by the fan used to pump the waste stream.

The fraction of the cross-section of the rotor for the cleaning steps was set to $f_C = 0.02$.

The results (Luzi, 2015) are given in Table 4, where W_I is the mass of inert material and W_{act} is the mass of the inert matrix plus the mass of catalytic washcoat in the active central zone,

$$W_I = V f_I[\rho_I(1-\varepsilon)] \tag{26}$$

$$W_{act} = V(1-f_I)[\rho_{cat} a_v \ell + \rho_I(1-\varepsilon-a_v\ell)], \tag{27}$$

where $\rho_I = 2511$ kg m^{-3} and $\rho_{cat} = 2745$ kg m^{-3}. The values of W_I and W_{act} are similar as the same volume fraction of the inert and active material was set ($f_I = 0.5$).

The values $t_{cycle,low}$ and $t_{cycle,crit}$ in Table 4 defines the practical operating range of the RRFR when fed with the nominal VOC concentration. The minimum value $t_{cycle,low}$ is restricted by a maximum allowed temperature of the catalyst $T^{adm}_{S,\max} = 400$ °C, a value that is a tentative temperature for avoiding a fast deactivation rate of the catalyst. Presently, we have no information about the actual thermal stability of the catalyst under consideration, but regarding that the active material is an oxide mixture, such a temperature level was chosen as a conservative value. On the other hand, the maximum value $t_{cycle,crit}$ is that value at which the ignited steady state is no longer sustained.

A remarkable feature of the reverse flow operation is its ability to auto-regulate the temperature of the system to compensate for the progressive decay of the catalytic activity. This can be explained by considering that each slice of the catalytically active material can also participate in the heat regeneration mechanism, if the catalytic ignition temperature has not been reached. Therefore, when the catalyst activity decays, a greater amount of catalytic material will be only involved in the heat regeneration process and thus higher temperatures can be reached to allow high reaction rates (see e.g. Eigenberger and Nieken, 1988; Matros, 1989).

It is therefore relevant to evaluate the critical catalytic activity ratio a_{crit}/a_0 leading to the reactor extinction for the design of the RRFR summarized in Table 4, operated with the minimum VOC concentration and $t_{cycle} = t^{\min}_{cycle}$. To this end, it was assumed that the three reaction rates (Eq. (1)) are affected by the same deactivation factor a/a_0. The resulting value $a_{crit}/a_0 = 0.081$ confirms the strength of the self-regulation mechanism.

5. Design and operation of the RHE-SR for the comparison with the RRFR

The first step in the design of the RHE-SR was also the choice of the monolith cell from the list in Table 3. As explained in detail by Luzi (2015), the necessary masses of regenerator and catalytic reactor, and the range of cycle times in which an ignited steady state is feasible at nominal VOC concentration were taken as criteria for the selection. Cell #2 arose as the best choice and it has been retained for further analysis unless otherwise stated.

Table 4
Resulting dimensions for the RRFR for the monolith cell #5.

V (m^3)	L (m)	D (m)	W_I (kg)	W_{act} (kg)	Re	$t_{cycle,low}$ (s)	$t_{cycle,crit}$ (s)
1.54	0.485	2.01	622	628	263	66	152

As for the operation of the RRFR, values of t_{cycle} and $|\Delta P|$ were restricted to the minimum $t_{cycle}^{\min} = 30$ s and the maximum $|\Delta P|^{adm} = 50$ mbar, respectively.

Consider first the definition of the cleaning fraction f_C. Clearly, it is convenient to choose f_C as small as possible to allow most of the volume of the regenerator to be engaged in the heat regeneration process, but a large pressure drop in the cleaning step should be avoided. The value $f_C = 0.02$ was adopted in consideration of the values of the cleaning flow rate G_{mC} from Eq. (25) (note that the second equality in Eq. (25) reveals that G_{mC} is independent of f_C). In this way, the pressure drop in the cleaning step was always less than the value for the cooling step.

The most efficient thermal performance of the regenerator will be attained for similar fractions of the cooling and heat regeneration steps since the mass flow rates G_{mT} and $(G_{mT} + G_{mC})$, respectively, are practically equal. Then, the values $f_{cool} = 0.48$ and $f_{reg} = (1 - f_{cold} - f_C) = 0.5$ were chosen.

The sizing of the RHE-SR was undertaken on the same basis explained for the RRFR, i.e. operating at $t_{cycle} = t_{cycle}^{\min} = 30$ s with the minimum VOC concentration. Given the monolithic structure of both regenerator and catalytic reactor, the procedure to evaluate their volumes, V_{RHE} and V_R respectively, can be described independently of their length/diameter ratios, as discussed in Section 4. It was also explained in Section 4 that the design of the RRFR operated with the minimum VOC content and $t_{cycle} = t_{cycle}^{\min} = 30$ s allows to sustain an ignited steady state up to the point the catalytic activity reaches a critical ratio $a_{crit}/a_0 = 0.081$. Imposing the same behaviour at the same conditions to the RHE-SR appears to be a sound basis of comparison between both alternatives. This requirement will set a relationship between V_{RHE} and V_R. Thus, if V_{RHE} is small the stream entering the reactor will be poorly preheated and a large value of V_R will be necessary. Conversely, a large value V_{RHE} will allow a high value of the inlet reactor temperature, and a relatively small volume V_R will suffice to fulfil the requirement.

Accordingly, Fig. 3 shows values V_{RHE} and V_R and the inlet reactor temperature $T_G^{0,R}$. Values of $T_G^{0,R}$ less than about 240 °C lead to a fast increase of V_R. On the other hand, the saving rate of V_R begins to approach the rate of increase of V_{RHE} at temperatures higher than around 280 °C. The range 240 °C < $T_G^{0,R}$ < 280 °C seems to be reasonable for sizing the RHE-SR and it includes the condition $V_R = V_{RHE}$ (at about $T_G^{0,R} = 255$ °C), which matches the same ratio in the design of the RRFR (see Table 4). Therefore, as a further condition for comparison purposes, the restriction $V_R = V_{RHE}$ has been undertaken for the design of the RHE-SR.

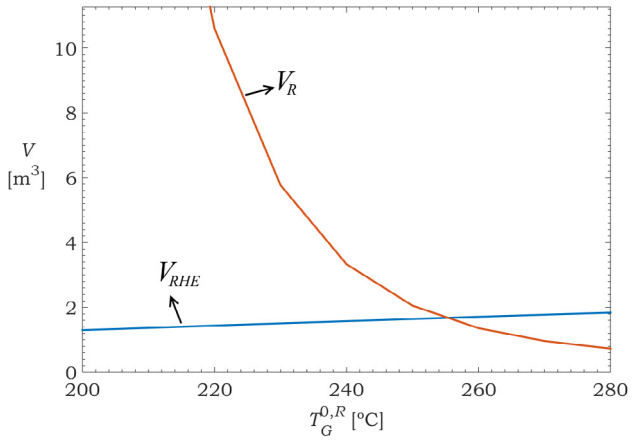

Fig. 3. Volumes required for the RHE and for the catalytic reactor for different values of $T_G^{0,R}$ for the minimum inlet VOCs concentration, $a_{crit}/a_0 = 0.081$ and $t_{cycle} = t_{cycle}^{\min} = 30$ s.

For given values of the volumes $V_{RHE} = \frac{\pi}{4} D_{RHE}^2 L_{RHE}$ and $V_R = \frac{\pi}{4} D_R^2 L_R$, it is necessary to define some criteria to establish the individual values D_{RHE}, D_R, L_{RHE} and L_R. In first place, as similarly employed for the RRFR, the overall pressure drop is fixed by $|\Delta P|^{adm} = 50$ mbar when the RHE-SR operates at a maximum allowed temperature, $T_{S,\max}^{adm}$. As pressure drop increases with the kinematic viscosity μ_G/ρ_G and this does with temperature, the evaluation at $T_{S,\max}^{adm}$ guarantees that $|\Delta P|^{adm}$ will not be exceeded at any other operating conditions. The maximum temperature level in the RHE-SR is reached at the exit of the catalytic reactor ($T_{S,\max}$) and this was set at $T_{S,\max}^{adm} = 400$ °C. On the other hand, fixing the overall pressure drop to the maximum values $|\Delta P|^{adm}$ will lead to the lower values of the cross-section areas $S_{RHE} = \frac{\pi}{4} D_{RHE}^2$ and $S_R = \frac{\pi}{4} D_R^2$. This is desirable to reduce the cost of the vessels heads and, in addition, to facilitate a uniform flow distribution. Assuming that the regenerator and the reactor are housed in independent vessel and that the cost of the head are proportional to the corresponding cross-section areas, a second condition for evaluating the linear dimensions is that of a minimum for the sum $(S_R + S_{RHE})$. From the outlined procedure (details are given in Appendix B), the following expressions are obtained for equal volumes $V_R = V_{RHE} = V$:

$$D_{RHE} = 2.46 V^{1/4} \tag{28}$$

$$D_R = 2.11 V^{1/4} \tag{29}$$

As just described, the dimensions of the regenerator and the catalytic reactor become determined from the operation at minimum VOC concentration. The operation at higher VOC concentrations will be favourable as higher temperature in the catalytic reactor will be reached and consequently the regenerator will operate with higher driving forces. In practice, at each level of VOC concentration, there will be a practical range of cycle times to operate the system. The lower limit $t_{cycle,low}$ will be determined either by the imposed operating minimum $t_{cycle}^{\min} = 30$ s or by the value leading to the maximum allowed temperature ($T_{S,\max}^{adm} = 400$ °C), whichever is greater. The upper limit $t_{cycle,crit}$ of the range is the maximum value at which an ignited steady state is feasible. The range $\Delta t_{oper} = t_{cycle,crit} - t_{cycle,low}$ is most significant, since a large value will improve the controllability of the operation, will enable the system to deal with a wider range of the conditions and/or fluctuations of the waste stream (temperature, flow rate, relation between concentration of the different VOC) and with changes in catalytic performance. Besides, a large range will increase the probability to cope with shortcomings in the design of the unit. Therefore, values of $t_{cycle,crit}$ and $t_{cycle,low}$ have been evaluated at the nominal VOC concentration and fresh-catalyst activity $(a/a_0 = 1)$ for further comparison between the RHE-SR and RRFR systems.

A flowchart showing the sequence of calculations for setting the dimensions of the RHE-SR (at minimum VOC concentration) and values of $t_{cycle,crit}$ and $t_{cycle,low}$ at nominal VOC concentration is given in Fig. 4. The minimum and nominal VOC mole fractions in the waste stream are identified as $y_{j,G}^{0,\min}$ and $y_{j,G}^{0,nom}$, respectively. In addition, ε_a and ε_T are the absolute tolerances adopted for the catalyst activity $(5 \cdot 10^{-4})$ and maximum bed temperature (1 °C), respectively.

The loop in Fig. 4 for the operation at minimum VOC concentration leads to evaluate iteratively the values $V_{RHE} = V_R$ that satisfy $a_{crit}/a_0 = 0.081$. Although it is not made explicit in the diagram, at each trial value $V_{RHE} = V_R$ the relations in Eqs. (28) and (29) are used to evaluate the individual values D_{RHE}, L_{RHE}, D_R and L_R, and

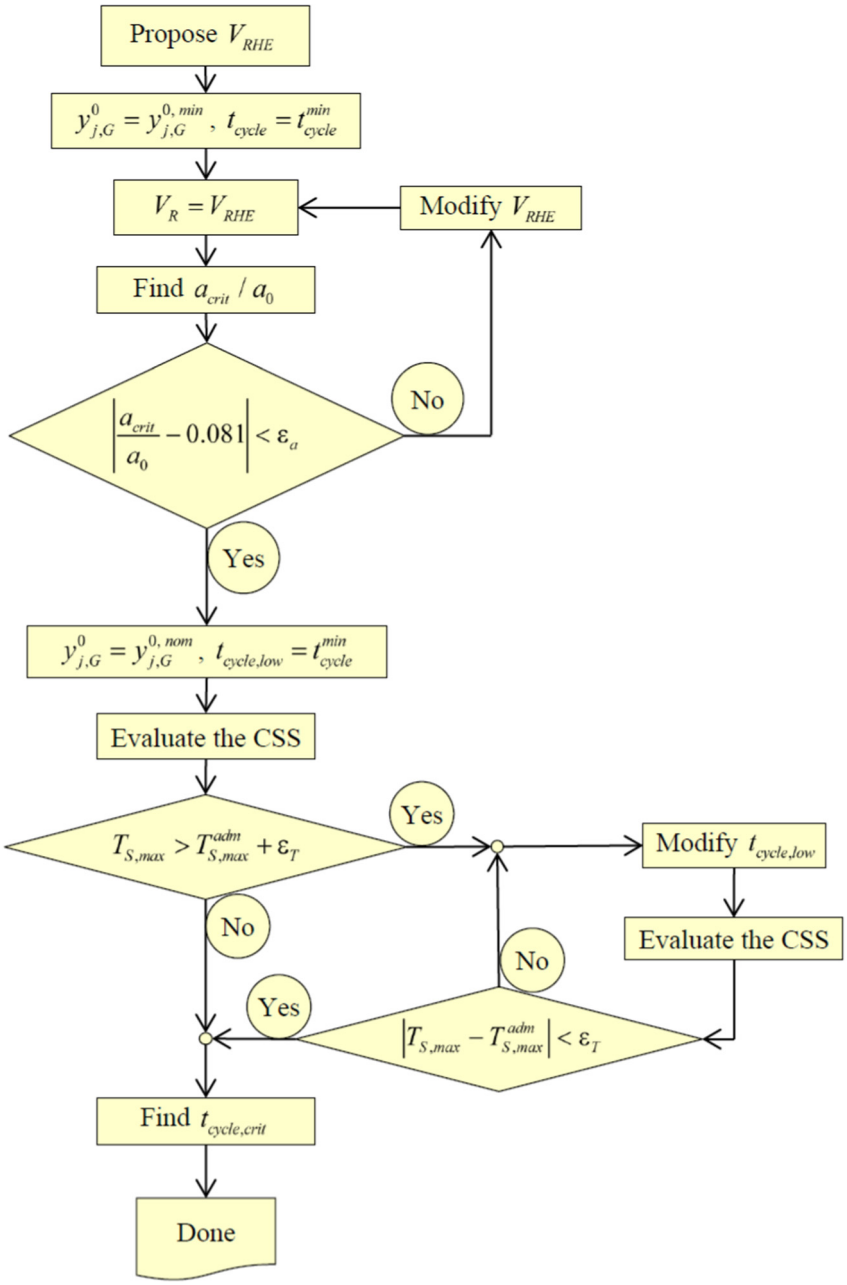

Fig. 4. Flowchart of the design strategy proposed.

with them the corresponding values of heat and mass transfer coefficients.

It should be also mentioned that the blocks "Find a_{crit}/a_0" and "Find $t_{cycle,crit}$" involves a trial and error search that requires the evaluation of the regenerator CSS in each step.

In order to visualize the results from these blocks, consider first the evaluation of a_{crit}/a_0. Fixing $t_{cycle} = t^{\min}_{cycle}$ and minimum VOC content, it can be assumed for trial values $V_{RHE} = V_R$ that the relation between ΔT^R and $T^{0,R}_G$ is found from solving only the CSS of the regenerator for a set of values of ΔT^R (see "alternative 2" in Section 3.2.1). The catalytic reactor operating at a certain value a/a_0 is simulated independently for a set of values $T^{0,R}_G$. A second relation between ΔT^R and $T^{0,R}_G$ can be evaluated in this way. If we plot the relations ΔT^R vs. $T^{0,R}_G$ obtained from the regenerator and from the reactor, the intersections of both curves determine the possible steady states of the RHE-SR.

Plots of this type are shown in Fig. 5a for the fresh catalyst ($a/a_0 = 1$) and for the critical activity $a_{crit}/a_0 = 0.081$ (see the figure inset for details). The corresponding VOC concentrations at the reactor exit as a function of $T^{0,R}_G$ are shown in Fig. 5b, where the close and open circle on each curve indicates the operations points (see the figure inset again for details). Only one curve ΔT^R vs. $T^{0,R}_G$ from the regenerator applies since it only depends on t_{cycle} for a given value of V_{RHE}. The curvature of this relationship is mainly due to the dependency of the air thermal conductivity with temperature. In turn, the decreasing values of ΔT^R at high values of $T^{0,R}_G$ in the curve from the reactor simulation arise mainly because of the dependency of the air specific heat with temperature. The behaviour depicted in Fig. 5a is very much like the familiar behaviour of autothermal systems composed of an adiabatic reactor and an external recuperative (stationary) heat exchanger.

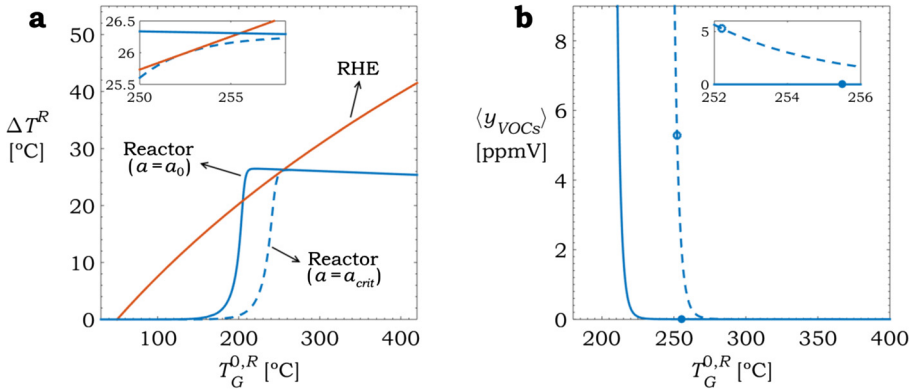

Fig. 5. (a) Operation curves in the RHE-SR for the minimum inlet VOCs concentration for the regenerator and for the reactor (solid line: fresh catalyst, dashed line: critical activity, $a_{crit}/a_0 = 0.081$). (b) VOC emission from the system (solid line: fresh catalyst, dashed line: critical activity; closed circle: operation point for the fresh catalyst, open circle: operation point for the critical activity).

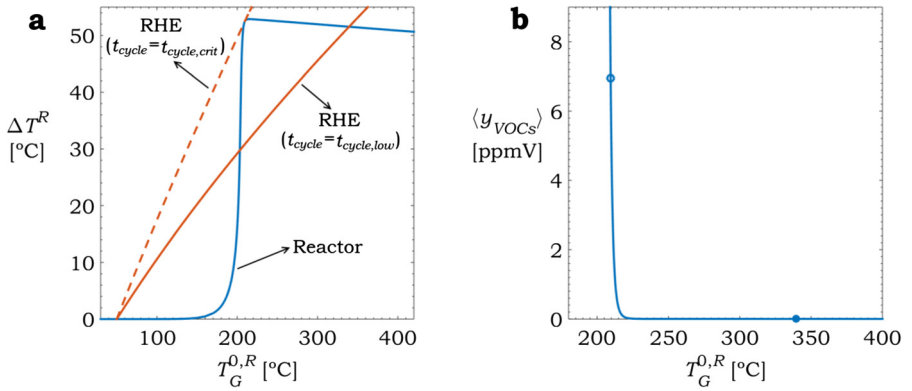

Fig. 6. (a) Operation curves in the RHE-SR for the nominal inlet VOC content for the regenerator (solid line: $t_{cycle} = t_{cycle,low}$, dashed line: $t_{cycle} = t_{cycle,crit}$) and for the catalytic reactor with $a/a_0 = 1$. (b) VOC emission from the system (closed circle: operation point for $t_{cycle} = t_{cycle,low}$, open circle: operation point for $t_{cycle} = t_{cycle,crit}$).

Table 5
Resulting dimensions for the RHE-SR for the monolith cell #2.

V_{RHE} (m^3)	L_{RHE} (m)	D_{RHE} (m)	V_R (m^3)	L_R (m)	D_R (m)	W_I (kg)	W_{act} (kg)	Re_{RHE}	Re_{RHE}	$t_{cycle,low}$ (s)	$t_{cycle,crit}$ (s)
1.68	0.273	2.80	1.68	0.366	2.42	1173	1183	314	210	70	110

Although three reactions take place in the present system, only up to three steady states (with the intermediate one being unstable) have been detected, in a similar way as for a single reaction (e.g. for the case $a/a_0 = 1$ in Fig. 5). This feature is mainly owing to the three reactions are activated in ranges of temperatures that are not separated enough from each other. The case with $a/a_0 = a_{crit}/a_0 = 0.081$ in Fig. 5a illustrates the solution for the search in the loop for minimum VOC content in Fig. 4, i.e. when the values $V_{RHE} = V_R$ are such that the system with catalytic activity $a/a_0 = 0.081$ operates just at the extinction point.

In a similar way, Fig. 6a and b illustrates the solution in the block "Find $t_{cycle,crit}$". In this case the curve ΔT^R vs. $T_G^{0,R}$ from the reactor simulation remains fixed ($a/a_0 = 1$ and nominal VOC content) and the regenerator is assumed to operate at different values of t_{cycle}. In Fig. 6a, the curves ΔT^R vs. $T_G^{0,R}$ from the CSS of the regenerator at $t_{cycle} = t_{cycle,low}$ and just at the searched value $t_{cycle} = t_{cycle,crit}$ are plotted.

The relevant results from the procedure sketched in Fig. 4 for the RHE-SR using cell#2 are given in Table 5. The mass of the inert material W_I in the regenerator and the total mass (inert matrix and catalytic washcoat material) W_{act} in the reactor are calculated as

$$W_I = V_{RHE}\rho_I(1-\varepsilon) \tag{30}$$

$$W_{act} = V_R[\rho_{cat}a_v\ell + \rho_I(1-\varepsilon-a_v\ell)] \tag{31}$$

6. Comparison between the results for the RRFR and RHE-SR systems

The differences between the designs and operating conditions of the RRFR and RHE-SR systems can be mainly discussed with the help of Tables 4 and 5 for the cells selected in each case.

Tables 4 and 5 clearly show that the sum of volumes of the inert (regenerator) and catalytically active monolithic structures required by the RHE-SR is substantially greater (118%) than the overall volume of the RRFR. As expected, the masses of solids in both units are correlated with the volumes, being the mass of the RHE-SR 88% greater. Those differences in volume and mass will have a significant impact on the investment cost for each alternative, because of the monolithic structures and also because of the size of the containers (see, in particular, the difference in diameters in Table 4 and 5).

The size of the RHE-SR arises from the requirement of an ignited steady state when the system is operated at minimum VOC content with the same level of catalyst deactivation tolerated by the RRFR, $a_{crit}/a_0 = 0.081$. The cause for the resulting difference in size is the ability of the RRFR to involve part of the deactivated catalyst in the heat exchange mechanism and in this way to automatically preheat the stream at higher temperatures. Instead, the stationary reactor of the RHE-SR system is unable to behave similarly and catalyst deactivation should be compensated with a significantly larger size of the unit.

It could be reasoned that the large size of the RHE-SR will provide flexibility of the operation, in particular regarding the range of cycle times that permits an operation at the ignited steady state. As discussed in Section 5, this feature can be appraised by the difference $\Delta t_{oper} = t_{cycle,crit} - t_{cycle,low}$, specifically evaluated at conditions of nominal VOC content and $a = a_0$. However, rather unexpectedly, Tables 4 and 5 show that Δt_{oper} for the RRFR is 115% wider. The difference is mainly due to the higher upper limit $t_{cycle,crit}$ allowed by the RRFR, a fact that again can be explained by the ability of the catalytic region to participate effectively in the regenerative heat exchange mechanism. As regards the lower limit $t_{cycle,low}$, the values are similar and in both cases restrained by the condition $T_{S,\max} = T^{adm}_{S,\max}$ = 400 °C.

The previous comparison between the RHE-SR and RRFR systems has been carried out for monolith cells independently chosen for each alternative, as explained in Section 4 and 5. It is then relevant to carry out a similar comparison for the same cell, as this will provide a different and valid frame of comparison. To this end, the results for the RRFR with cell #2 (the one previously chosen for the RHE-SR system) are presented in Table 6 for their comparison with the results in Table 5. It should be mentioned that the value of a_{crit}/a_0 for the design with the cell #2 was 0.080, being practically equal to the value found for the cell #5.

The difference between the sizes of the units is smaller in this case, although the total volume required by the RHE-SR is still 53% greater. The relatively larger size of the RRFR using cell#2 presents as an advantageous consequence the enlargement of Δt_{oper} (see Tables 4 and 6). In this way, the difference in Δt_{oper} between the RRFR and the RHE-SR using cell #2 in both cases increases to 220%.

The results from the present study indicate conclusively that a catalytic combustor for the treatment of VOC operated under the principle of flow reversal - in the present case the RRFR system- shows inherent advantages over a system combining a regenerative heat exchanger and a stationary catalytic combustor, RHE-SR. The relevant feature is posed by the ability of the catalytically active material in the flow reversal system to participate in the regenerative heat exchange mechanism.

Nonetheless, we understand that the use of the RHE-SR cannot be ruled out without due consideration of the specific application. It this sense, it should be emphasized that at the outside of this study we have decided to carry out the comparison under variable operating conditions, as regards the state of catalyst activity and a range of VOC concentrations in the waste stream. Also, the analysis was subject to the choice of some fixed levels for the imposed restrictions (i.e. available driving pressure, maximum allowable temperature, minimum cycle time, minimum catalyst activity). Clearly, a different frame of comparison can change in some degree the results here reported. Also, the fact that both units in the RHE-SR systems, regenerative heat exchange and catalytic reactor, can be independently supplied and installed may provide eventually an advantage. The type of materials and configuration of the solid matrix in both units can be different and their relative sizes can be optimized on the basis of investment and operating costs. Finally, technological details should be accounted for.

7. Conclusions

Two auto-thermal systems for the catalytic incineration of an air effluent contaminated with ethyl acetate and ethanol were analysed and compared: a rotary reverse flow reactor (RRFR) and a system comprising a rotary regenerative heat-exchanger (regenerator) and a stationary catalytic reactor (RHE-SR system). The RRFR, the regenerator and the stationary catalytic reactor were assumed to be monolithic structures with squared channels, and a small fraction (2%) of the cross-section areas of the RRFR and of the regenerator was employed to sweep de residual VOC in the channels before the flow reversal. The study was carried out by means of the mathematical simulation of the operation, for which a one-dimensional model, based on the assumption of negligible transversal heat conduction, was employed.

In first place, five configurations of the monolith cell were considered and one of them was selected as the best one for each setup, according to the criteria and details reported by Luzi (2015). The selected cells were different for both systems.

The dimensions of the RRFR and operating values of the cycle time were then evaluated, as reported by Luzi et al. (2016), and summarized in the present contribution. This was carried out by considering that the VOC content in the waste stream can vary between nominal and minimum levels and imposing a number of restrictions such as available pressure drop, maximum allowable temperature, minimum cycle time and emission limit value. Setting the same volumes of inert and catalytically active materials was found to be suitable as an additional design criterion. The actual concentration of unburned VOC were always significantly lower than the emission limit value (20 mgC/Nm^3), except when the system closely approaches the extinction, which is definitely an unsuitable operating condition. The minimum catalyst activity to sustain an ignited steady state was also considered as a relevant feature. The design of the RRFR tolerates a decay of the catalyst activity of around 92% with respect to the fresh catalyst.

The design of the RHE-SR was undertaken by considering similar constraints as for the RRFR. In addition, the same level of allowable catalyst deactivation as in the RRFR and equal volumes of regenerator and catalytic reactor was imposed.

The design of both autothermal systems were compared on the basis of their sizes and the feasible ranges of cycle time (Δt_{oper}) that is the only operative variable that, in practice, can be manipulated in both systems. The results showed conclusive advantages in favour of the RRFR, as the required volume and mass of solid materials (inert and catalyst) was around half the values involved in the RHE-SR system and Δt_{oper} was 115% wider. Since these results were obtained with different types of cells for each alternative, an additional comparison was made with the RRFR employing the same cell selected for the RHE-SR. In this case the design RRFR required more solid materials, but still the volume and mass were 2/3 of the values for the RHE-SR. On the other hand, the difference in the range of Δt_{oper} increased to 220%.

Table 6
Resulting dimensions for the RRFR for the monolith cell #2.

V (m^3)	L (m)	D (m)	W_I (kg)	W_{act} (kg)	Re	$t_{cycle,low}$ (s)	$t_{cycle,crit}$ (s)
2.20	0.729	1.96	766	773	328	58	186

It was concluded that the main reason for the higher efficiency of the RRFR is the ability of the catalytically active material in a flow reversal system to participate in the regenerative heat exchange mechanism, a feature that is precluded by the stationary behaviour of the catalytic reactor in the RHE-SR system.

Acknowledgements

The authors wish to thank the financial support of the following Argentine institutions: ANPCyT-MINCyT (PICT'15 - 3546), CONICET (PIP 0018), and UNLP (PID 11/I177). O. M. Martínez and G. F. Barreto are Research Members of CONICET. C. D. Luzi, holds a grant from CONICET.

Appendix A. Validity of uniform flow distribution and negligible heat conduction effects on transverse directions

A.1. Negligible heat conduction effects on transverse directions

Disregarding axial and radial thermal conduction, the amounts of heat exchanged between the monolith walls and the fluid flow and the heat released by the catalytic reactions are either accumulated by the solid walls or angularly conducted. A suitable thermal Peclet number based on a half-cycle (i.e. for a reaction step in the RRFR or for a cooling/heat regeneration step in the rotor of the RHE-SR) to assess the relative magnitudes of both mechanisms can be defined in the way

$$Pe_{tang} = \frac{(\pi r)[(1-\varepsilon)(\rho c_p)_S]u_{tang}}{\lambda_{ef,trans}} \quad (A.1)$$

where r is the radial coordinate, (πr) is the arch length in a half-cycle, $u_{tang} = 2\pi\, r/t_{cycle}$ is the tangential velocity and $\lambda_{ef,trans}$ is the transversal effective thermal conductivity of the matrix evaluated as: $\lambda_{ef,trans} \approx \frac{\lambda_S}{(1-\varepsilon^{1/2})+\left(\frac{1-\varepsilon^{1/2}}{\varepsilon^{1/2}}+\mathrm{Nu}\frac{\lambda_G}{\lambda_S}\right)^{-1}}$.

Pe_{tang} reaches a value of approximately 7700 for a cycle time of 100 s and a radial position, r, of 0.1 m, which is much less than rotor radii resulting in the designs considered in Sections 4 and 5. Thus, it can be certainly expected that the transversal heat conduction will have negligible impact on the operation of any of the setups. In this sense, a simplified evaluation was carried out at the boundary of the rotor, where the strongest impact of angular conduction is expected due to the sudden change of fluid temperature when the fluid flow is reversed. The largest difference found between the dimensionless temperature profiles when including or neglecting the angular conduction was of the order of $3 \cdot 10^{-3}$ (just at the point of flow reversal), which reflects the high Peclet number discussed above and confidently allows neglecting angular conduction effects (details of this evaluation will be willingly provided by the corresponding author by request).

A.2. Uniform flow distribution

It is assumed that the design of the feeding compartments allows a uniform distribution of flow in the available channels of the rotor, either in the RRFR or in the regenerator of the RHE-SR. However, the temperature profile inside the channel varies with the time each channel has spent in a given step. Then, hotter channels aligned on the same radius will admit lower mass flow rates, under the requirement of the same pressure drop in all channels in the same step. To check if the assumption of uniform flow distribution is correct, we have first focused on the behaviour of the RHE-SR. The conservation equations described in Section 3.2, along with initial and boundary condition in Section 3.2.1, were solved for the design conditions reported on Section 5, but considering that the test channel after spending a time t in a given step (cooling, cleaning or heat regeneration), or alternately, after spanning an angle $\phi = (2\pi)t/t_{cycle}$, is fed with a superficial mass velocity $G(\phi)$, evaluated from the instantaneous temperature profile and globally restrained to the mass flow rate fed in each step.

The results obtained once the CSS is reached are compared with those employing the assumption of uniform flow distribution in Fig. A.1. It can be appreciated in Fig. A.1 that $G(\phi)$ in the cooling step varies significantly and that the effect is enhanced for longer

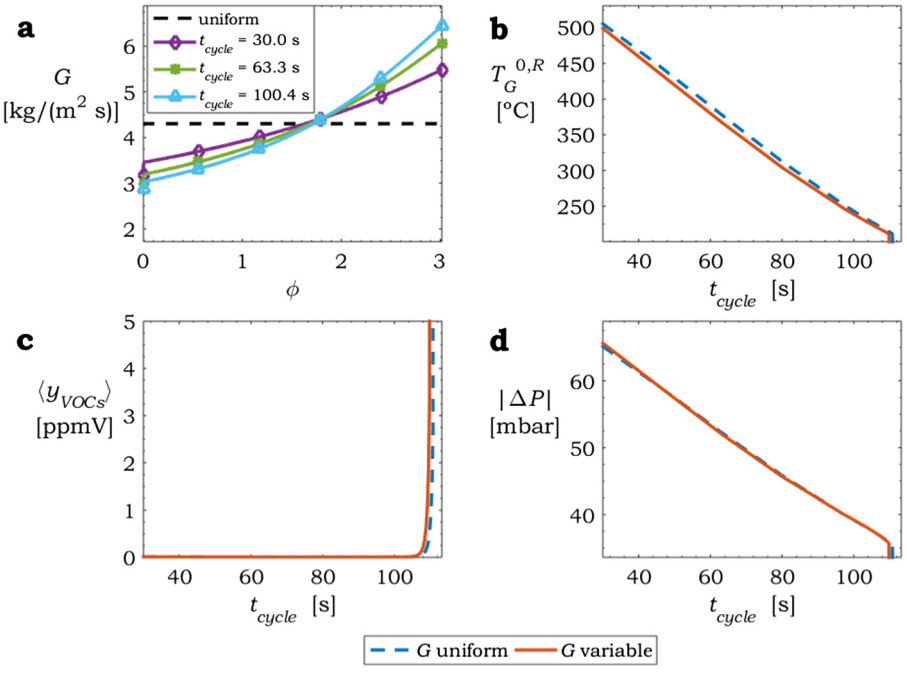

Fig. A.1. Influence of the inlet mass flow rate variation on the angular position. (a) Dependence of the superficial mass velocity, G, with the angular position, ϕ, for the cooling step. (b–d) Effect of the variation of the superficial mass velocity on the CSS of the entire system RHE-SR.

cycle times, as greater temperature differences arise in this way. However, the relevant variables in the operation of the RHE-SR, inlet temperature to the catalytic reactor $T_G^{0,R}$, the total emission of VOCs $\langle y_{VOCs}\rangle$, and the total pressure drop on the system $|\Delta P|$ (Fig. A.1b–d) hardly differ from the values using a uniform flow distribution, even when the extinction of the ignited cyclic steady sate is approached (Fig. A.1c). It can be safely concluded that the assumption of uniform flow distribution is suitable for the correct description of the RHE-SR, in spite of significant variation of $G(\phi)$ with ϕ. Actually, the conclusion is in line with the procedures recommended for the analysis of rotary regenerators in the specific bibliography (e.g. Shah and Sekulić, 2003; Thulukkanam, 2013; Willmott, 2002)

Turning to the case of the RRFR, a channel during a cycle is subject to two equivalent reaction steps and two cleaning steps. As the cleaning steps are much shorter, the temperature profile remains practically unchanged and hence the incoming cleaning stream can be confidently assumed to be uniformly distributed. As regards a reaction step, once the CSS is reached, the temperature profiles in the first half of the step will very approximately mirror the profiles in the second half. Then, the changes in the mass velocity will only take place during nearly a quarter of a cycle. Moreover, in this period, the mean temperature in the channel does not suffer large variations, as the heat accumulated in the walls is "pushed" from one side of channel to the other. From the temperature profiles obtained by employing the assumption of uniform flow distribution in the CSS, we have estimated that the maximum difference in pressure drop is only less than 6% and the mass velocity in the channels will approximately vary in the same proportion. The impact of this variation on the overall behaviour of the RRFR is therefore expected to be almost negligible.

Appendix B. Determination of cross-section areas S_R and S_{RHE} in the RHE-SR system

For given values of the volumes $V_{RHE} = S_{RHE}L_{RHE}$ and $V_R = S_R L_R$ in the RHE-SR system, the overall pressure drop is set at the value $|\Delta P|^{adm}$ allowed for the blower. Considering that the cleaning flow rate is approximately three orders of magnitude lower than the total flow rate, it is neglected for evaluating the pressure drop at this instance (i.e. in the heat regeneration step and in the catalytic reactor).

The individual pressure drops in the cooling and heat regeneration steps of the regenerator are evaluated by assuming constant values of the kinematic viscosity $\nu_G = \mu_G/\rho_G$ evaluated at the average temperature, $\langle T\rangle$, and pressure, $\langle P\rangle$, in each step. From the Fanning equation,

$$|\Delta P_{RHE}| = \gamma G_{mT}\frac{\nu_{RHE}V_{RHE}}{S_{RHE}^2} \tag{B.1}$$

where $\gamma = \frac{1}{8}(fRe)\frac{a_v^2}{\varepsilon^3}$, $\nu_{RHE} = \frac{\nu_{cool}}{f_{cool}} + \frac{\nu_{reg}}{f_{reg}}$ and ν_{cool}, ν_{reg} are the kinematic viscosities in the cooling and heat regeneration steps.

In a similar way, for the catalytic reactor:

$$|\Delta P_R| = \gamma G_{mT}\nu_R\frac{V_R}{S_R^2}, \tag{B.2}$$

Setting $|\Delta P|^{adm} = |\Delta P_{RHE}| + |\Delta P_R|$:

$$|\Delta P|^{adm} = \gamma G_{mT}\left[\frac{\nu_{RHE}V_{RHE}}{S_{RHE}^2} + \frac{\nu_R V_R}{S_R^2}\right], \tag{B.3}$$

As was discussed in Section 5, an additional criterion to evaluate S_{RHE} and S_R arises by imposing a minimum for the sum $(S_{RHE} + S_R)$. That is, after differentiating Eq. (B.3) with respect to S_{RHE} and S_R, while considering all the remaining parameters as constants, and taking $dS_R = -dS_{RHE}$:

$$\frac{\nu_{RHE}V_{RHE}}{S_{RHE}^3} = \frac{\nu_R V_R}{S_R^3} \tag{B.4}$$

After replacing alternatively either S_{RHE} or S_R from Eq. (B.4) in Eq. (B.3), it is obtained

$$S_{RHE}^2 = \gamma G_{mT}\frac{\nu_{RHE}V_{RHE}}{|\Delta P|^{adm}}\left[1 + \left(\frac{\nu_R V_R}{\nu_{RHE}V_{RHE}}\right)^{1/3}\right] \tag{B.5}$$

$$S_R^2 = \gamma G_{mT}\frac{\nu_R V_R}{|\Delta P|^{adm}}\left[1 + \left(\frac{\nu_{RHE}V_{RHE}}{\nu_R V_R}\right)^{1/3}\right] \tag{B.6}$$

For evaluating the kinematic viscosities ν_{cool}, ν_{reg} and ν_R, the absolute pressure was taken in all cases as $\langle P\rangle = P^0 - |\Delta P|^{adm}/2$, and the average temperatures were calculated as

$$\langle T\rangle_{cool} = [T_G^0 + \left(T_{S,\max}^{adm} - \Delta T_{ad}\right)]/2, \tag{B.7}$$

$$\langle T\rangle_{reg} = [(T_G^0 + \Delta T_{ad}) + T_{S,\max}^{adm}]/2, \tag{B.8}$$

$$\langle T\rangle_R = T_{S,\max}^{adm}, \tag{B.9}$$

where the temperature rise in the reactor is assumed to be ΔT_{ad} and $T_{S,\max}^{adm}$ is reached at the reactor outlet. In the cooling and heat regeneration steps the average temperature is taken as the arithmetic mean between inlet and outlet values. The average reactor temperature is taken approximately as $T_{S,\max}^{adm}$, considering the usual case in which the conversion of VOC takes place rapidly close to the reactor inlet and, consequently, most of the reactor length remains at $T_{S,\max}^{adm}$.

Taking the values $T_G^0 = 50\,^\circ C$, $\Delta T_{ad} = 54\,^\circ C$ (for the nominal VOC concentration) and $T_{S,\max}^{adm} = 400\,^\circ C$ (see Section 5), the values $\langle T\rangle_{cool}$, $\langle T\rangle_{reg}$ and $\langle T\rangle_R$ in Eqs. (B.7)–(B.9) and, consequently, ν_{cool}, ν_{reg} and ν_R become defined. In addition, $G_{mT} = 12.7\ kg\ s^{-1}$ (Table 1), $(fRe) = 14.2$ for square channels in laminar regime, $a_v = 2677\ m^{-1}$, $\varepsilon = 0.722$ for Cell #2 (Table 3), $|\Delta P|^{adm} = 50$ mbar (Section 5). Thus, all values necessary to relate the cross-section areas to the volumes in Eqs. (B.5) and (B.6) are defined. By writing $S_{RHE} = \frac{\pi}{4}D_{RHE}^2$ and $S_R = \frac{\pi}{4}D_R^2$, and taking $V_{RHE} = V_R = V$ as assumed in Section 5, Eqs. (28) and (29) in the main text arise from Eqs. (B.5) and (B.6).

References

Boger, T., Heibel, A.K., Sorensen, C.M., 2004. Monolithic catalysts for the chemical industry. Ind. Eng. Chem. Res. 43, 4602–4611. http://dx.doi.org/10.1021/ie030730q.

Campesi, M.A., Luzi, C.D., Martínez, O.M., Barreto, G.F., 2012a. Effect of concentration by thermal swing adsorption on the catalytic incineration of VOCs. Int. J. Chem. React. Eng. 10. http://dx.doi.org/10.1515/1542-6580.3026.

Campesi, M.A., Mariani, N.J., Bressa, S.P., Pramparo, M.C., Barbero, B.P., Cadús, L.E., Barreto, G.F., Martínez, O.M., 2012b. Kinetic study of the combustion of ethanol and ethyl acetate mixtures over a MnCu catalyst. Fuel Process. Technol. 103, 84–90. http://dx.doi.org/10.1016/j.fuproc.2011.08.019.

Chen, G., Chi, Y., Yan, J., Ni, M., 2011. Effect of periodic variation of the inlet concentration on the performance of reverse flow reactors. Ind. Eng. Chem. Res. http://dx.doi.org/10.1021/ie102342w.

Directive 2010/75/EU of the European Parliament and of the Council - on industrial emissions (integrated pollution prevention and control) [WWW Document], 2010. Dir. 2010/75/EU. URL <http://data.europa.eu/eli/dir/2010/75/2011-01-06> (accessed 12.21.16).

Eigenberger, G., Nieken, U., 1988. Catalytic combustion with periodic flow reversal. Chem. Eng. Sci. 43, 2109–2115. http://dx.doi.org/10.1016/0009-2509(88)87091-X.

Fissore, D., Barresi, A.A., 2002. Comparison between the reverse-flow reactor and a network of reactors for the oxidation of lean VOC mixtures. Chem. Eng. Technol. 25, 421–426. http://dx.doi.org/10.1002/1521-4125(200204)25:4<421::AID-CEAT421>3.0.CO;2-K.

Gulati, S., 2005. Ceramic catalyst supports for gasoline fuel. In: Cybulski, A., Moulijn, J.A. (Eds.), Structured Catalysts and Reactors, pp. 21–70. http://dx.doi.org/10.1201/9781420028003.pt1.

Kolaczkowski, S., 2005. Treatment of Volatile Organic Carbon (VOC) Emissions from Stationary Sources, pp. 147–170. doi:http://dx.doi.org/10.1201/9781420028003.ch5.

Kolios, G., Frauhammer, J., Eigenberger, G., 2000. Autothermal fixed-bed reactor concepts. Chem. Eng. Sci. 55, 5945–5967. http://dx.doi.org/10.1016/S0009-2509(00)00183-4.

Luzi, C.D., 2015. Combustión catalítica de compuestos orgánicos volátiles utilizando sistemas autotérmicos con intercambio de calor regenerativo. Universidad Nacional de La Plata.

Luzi, C.D., Martínez, O.M., Barreto, G.F., 2016. Autothermal reverse-flow reactors: design and comparison of valve-operated and rotary systems. Chem. Eng. Sci. 148, 170–181. http://dx.doi.org/10.1016/j.ces.2016.03.033.

Marín, P., Ordóñez, S., Díez, F.V., 2010. Monoliths as suitable catalysts for reverse-flow combustors: modeling and experimental validation. AIChE J. 56, 3162–3173. http://dx.doi.org/10.1002/aic.12215.

Matros, Y.S., 1989. Catalytic Processes Under Unsteady-State Conditions. Elsevier.

Matros, Y.S., Bunimovich, G.A., 1996. Reverse-flow operation in fixed bed catalytic reactors. Catal. Rev. 38, 1–68. http://dx.doi.org/10.1080/01614949608006453.

Matros, Y.S., Noskov, A.S., Zagoruiko, A.N., Gol'dman, O.V., 1994. Comparison of technological design of the catalytic processes under unsteady-state conditions. Theor. Found Chem. Eng. 28, 139–144.

Morales, M.R., Barbero, B.P., Cadús, L.E., 2008. Evaluation and characterization of Mn-Cu mixed oxide catalysts for ethanol total oxidation: influence of copper content. Fuel 87, 1177–1186. http://dx.doi.org/10.1016/j.fuel.2007.07.015.

Shah, R.K., Sekulić, D.P., 2003. Fundamentals of Heat Exchanger Design. John Wiley & Sons.

Thulukkanam, K., 2013. Heat Exchanger Design Handbook. CRC Press.

Vortmeyer, D., Schaefer, R.J., 1974. Equivalence of one- and two-phase models for heat transfer processes in packed beds: one dimensional theory. Chem. Eng. Sci. 29, 485–491. http://dx.doi.org/10.1016/0009-2509(74)80059-X.

Willmott, A.J., 2002. Dynamics of Regenerative Heat Transfer. Taylor & Francis.

Zagoruiko, A.N., 2012. The reverse-flow operation of catalytic reactors: history and prospects. Curr. Top. Catal. 10.